Multicoefficient Gaussian-3 Calculation of the Rate Constant for the OH + CH 4 Reaction and Its 12 C/ 13 C Kinetic Isotope Effect with Emphasis on the Effects of Coordinate System...

ARTICLE *in* THE JOURNAL OF PHYSICAL CHEMISTRY A · DECEMBER 2007

Impact Factor: 2.69 · DOI: 10.1021/jp072843j · Source: PubMed

5 AUTHORS, INCLUDING:

Benjamin A Ellingson
OpenEye Scientific Software
10 PUBLICATIONS **630** CITATIONS
SEE PROFILE

Jingzhi Pu
Indiana University-Purdue University Indiana...
41 PUBLICATIONS **3,899** CITATIONS
SEE PROFILE

Yan Zhao
Hewlett-Packard
80 PUBLICATIONS **21,113** CITATIONS
SEE PROFILE

Donald Truhlar
University of Minnesota Twin Cities
1,342 PUBLICATIONS **81,415** CITATIONS
SEE PROFILE

Multicoefficient Gaussian-3 Calculation of the Rate Constant for the OH + CH_4 Reaction and Its $^{12}C/^{13}C$ Kinetic Isotope Effect with Emphasis on the Effects of Coordinate System and Torsional Treatment

Benjamin A. Ellingson,[†] Jingzhi Pu,[‡] Hai Lin,[§] Yan Zhao,[†] and Donald G. Truhlar*,[†]

Department of Chemistry and Supercomputing Institute, University of Minnesota, 207 Pleasant Street Southeast, Minneapolis, Minnesota 55455-0431, Department of Chemistry and Chemical Biology, Harvard University, Cambridge, Massachusetts 02138, and Department of Chemistry, University of Colorado at Denver and Health Sciences Center, Denver, Colorado 80217

Received: April 12, 2007; In Final Form: July 9, 2007

Rate constants and $^{12}C/^{13}C$ kinetic isotope effects are calculated by direct dynamics for the OH + CH_4 → H_2O + CH_3 reaction. The electronic structure calculations required to generate the implicit potential energy surface were carried out by the high-level multicoefficient Gaussian-3/version-3 (MCG3) method and compared to two other multilevel methods, MC3BB and MC3MPW, and three density functional methods, M06-2X, BB1K, and MPW1K. The rate constants and $^{12}C/^{13}C$ kinetic isotope effects are shown to depend strongly on the coordinate system used to calculate the frequencies as well as on the method used to account for the torsional anharmonicity of the lowest-frequency vibrational mode of the generalized transition states.

1. Introduction

The reaction of OH with CH_4 is very important in the Earth's troposphere, accounting for 90% ± 5% of the total sink of CH_4.[1] Uncertainty in the $^{12}C/^{13}C$ kinetic isotope effect (KIE) for this reaction can have a significant impact on the isotopic compositions in atmospheric models.[2] The $^{12}C/^{13}C$ KIE has been experimentally measured by Cantrell et al.[3] and Saueressig et al.,[4] yielding results of 1.0054 and 1.0039, respectively, at 296 K. Even this seemingly small difference in experimental measurements has an important impact on studies of the troposphere.[2,5] Furthermore, it is important to include the correct temperature dependence, which is not available from experiment, especially for the atmospherically important range of $T = 200-300$ K.

The $^{12}C/^{13}C$ KIE has been calculated several times.[6−8] It was first pointed out by the authors[7] and then confirmed by Sellevag et al.[8] that the $^{12}C/^{13}C$ KIE is very sensitive to the treatment of the torsional anharmonicity of the lowest-frequency vibrational mode. Furthermore, it was shown that certain methods for torsional anharmonicity could bring the calculated results into agreement with the experimental results for the levels of theory that were used for the potential energy surface (PES).

It has been known for over 60 years that the harmonic approximation may be seriously in error for hindered internal rotation,[9−11] also called torsion. The lowest-frequency vibrational mode of the OH plus CH_4 transition state corresponds to this type of motion, which can be conceptually described as the OH fragment rotating with respect to the CH_3 fragment. This particular type of torsion is the most troublesome for dynamics calculations because it occurs in the transition state but not in the reactants, so there is no possibility of a cancellation of error. Therefore, an accurate treatment of the torsional mode is very important for this type of reaction, especially when the KIE being calculated is only on the order of parts per thousand (ppt).

The KIE is determined in the present work by calculating the ratio of separately calculated rates, one for ^{12}C and the other for ^{13}C. The rate constants are calculated using variational transition state theory with multidimensional tunneling (VTST/MT),[12,13] specifically by canonical variational transition state theory with small-curvature tunneling (CVT/SCT).[12,13] The equation for the CVT rate constant is

$$k^{\mathrm{CVT}} = \frac{1}{h\beta}\frac{Q^{\mathrm{GT}}(T,s_*^{\mathrm{CVT}}(T))}{\Phi^{\mathrm{R}}(T)}\exp\{-\beta V_{\mathrm{MEP}}[s_*^{\mathrm{CVT}}(T)]\} \quad (1)$$

where $\beta = (k_B T)^{-1}$, k_B is Boltzmann's constant, T is the temperature, $Q^{\mathrm{GT}}(T, s_*^{\mathrm{CVT}})$ is the quantum mechanical quasi-partition function of the generalized transition state, $\Phi^{\mathrm{R}}(T)$ is the quantum mechanical partition function per unit volume for reactants, and $V_{\mathrm{MEP}}(s_*^{\mathrm{CVT}})$ is the potential energy difference between the reactants and the generalized transition state at $s = s_*^{\mathrm{CVT}}$, where s is the reaction coordinate specifying the location of the system on the minimum energy path (MEP) and s_*^{CVT} is the optimal location of the dividing surface along the MEP. The SCT contribution is included by a multiplicative factor, κ^{SCT}, which depends on the potential energy and on the frequencies along the MEP. Separate MEPs were calculated for the ^{12}C and ^{13}C systems by direct dynamics for each level of theory, where direct dynamics means[14−21] that each required energy, gradient, or Hessian is calculated as needed by electronic structure theory.

For a given level of electronic structure theory, the ^{12}C and ^{13}C systems have the same PES. However, the MEP used for CVT/SCT is determined as the path of steepest descent in isoinertial coordinates, also known as mass-scaled coordinates,[22] and therefore the MEPs are different for the ^{12}C and ^{13}C systems

* Author to whom correspondence should be addressed. E-mail: truhlar@umn.edu.
[†] University of Minnesota.
[‡] Harvard University.
[§] University of Colorado at Denver and Health Sciences Center.

10.1021/jp072843j CCC: $37.00
Published on Web 10/20/2007

because of the difference in mass for the carbon atom. Additionally, the eigenvectors associated with the imaginary frequency at the saddle point are not the same for the ^{12}C and ^{13}C systems because of the difference in mass. This eigenvector dictates the first step when constructing the MEP, and hence the MEPs for the ^{12}C and ^{13}C systems are different from the very first step. Therefore, wholly independent rate constants have been calculated for the ^{12}C and ^{13}C systems for each level of electronic structure theory.

This paper represents an advance over our preliminary communication[7] on this subject in two respects. First, we have now carried out the electronic structure calculations at a very high level, MCG3/3. This is probably the most complicated reaction ever studied by full direct dynamics with such a high level of electronic structure theory. Second, the present paper contains a much more thorough treatment of the torsional problem and coordinate systems, both of which have a significant effect on this very small kinetic isotope effect.

2. Computational Methods

2.1. Electronic Structure Methods. The levels of theory used in the present work are MCG3/3,[23,24] MC3BB,[25] MC3MPW,[25] MPW1K/MG3S,[26,27] BB1K/MG3S,[28] and M06-2X/MG3S.[29]

The MCG3/3, MC3BB, and MC3MPW methods are multilevel methods that combine several calculations to extrapolate toward an accurate result. The MCG3/3 extrapolation includes a QCISD(T)[30] calculation with the 6-31G(d) basis set[31] and an MP2[32] calculation with the MG3S basis set,[27] which makes it the highest level of theory used to study the $^{12}C/^{13}C$ KIE for OH plus CH_4. The application of such a high-level calculation for direct dynamics on a seven-atom system was a lengthy endeavor that was only feasible by using a supercomputer. The MC3BB and MC3MPW extrapolations are called doubly hybrid density functional theory,[25] and they use a combination of Hartree−Fock (HF) theory,[32] MP2, and density functional theory (DFT). The calculations employing multilevel methods were carried out using MULTILEVEL, version 4.2.[33]

MPW1K is a one-parameter hybrid density functional, and BB1K is a hybrid meta-density functional; in both of these functionals, the percentage of HF exchange has been parametrized for the calculation of accurate kinetics data (in particular barrier heights and energies of reaction). Calculations by these two methods were carried out using the *Gaussian 03* computer program.[34] M06-2X is a hybrid meta-DFT method with a high percentage of HF exchange;[29] it represents a refinement of the M05-2X functional.[35] The good success of this recently designed density functional makes it the recommended density functional method for kinetics.[29] For the present study, calculations employing the M06-2X method were carried out using the *Gaussian 03*-MN-GFM computer module,[36] which is a locally modified, undistributed (due to licensing restrictions) module of *Gaussian 03*.[34]

The barrier height and energy of reaction for each method have been tabulated and compared to Weizmann-1 (W1) theory[37] in Table 1. W1 is a very accurate and computationally expensive multilevel-type method developed by Parthiban and Martin,[37] and a W1 calculation by Boese and Martin[38] is the highest level of theory that has been used to determine the barrier height and energy of reaction for the OH + CH_4 system. A picture of the saddle point at the MCG3/3 level is given in Figure 1, which shows the atom numbering used in this article. Geometries for each species at each level of theory have been included in the Supporting Information.

2.2. Rate Constant Calculation. All rate constant calculations were performed with POLYRATE, version 9.6.[39] The multilevel methods were interfaced with POLYRATE via MULTILEVELRATE, version 9.4.[40] The DFT methods were interfaced with POLYRATE via GAUSSRATE, version 9.6.[41]

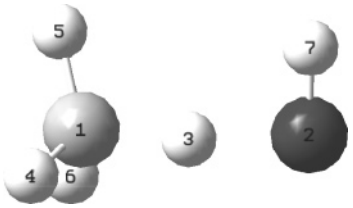

Figure 1. Picture of the CH_3-H-OH transition state with numbered atoms for the MCG3/3 level of theory.

TABLE 1: Barrier Heights ($V^{\ddagger}$) and Energy of Reaction (ΔE) for the OH + $CH_4 \rightarrow H_2O + CH_3$ Reaction

	$V^{\ddagger}$ (kcal/mol)	ΔE (kcal/mol)
W1[a]	6.22	−13.44
MCG3/3	6.35	−13.91
MC3BB	6.11	−11.81
MC3MPW	6.15	−12.63
M06-2X/MG3S	5.72	−12.04
BB1K/MG3S	6.81	−9.96
MPW1K/MG3S	7.28	−10.17

[a] From ref 38.

The MEP was calculated by the Euler steepest-descents method[42] with a step size of 0.00265 Å in isoinertial coordinates[22,43] scaled to a reduced mass of 1 amu, and a Hessian was calculated every 10 steps. This small step size was determined in a previous communication[7] by some preliminary DFT kinetics calculations designed to determine the numerical parameters needed to ensure convergence for the KIEs. (Convergence to a high precision is very important for the calculation of heavy-atom kinetic isotope effects because they are so close to unity.)

The rotational symmetry numbers for CH_4, OH, and the CH_3-H-OH transition states are 12, 1, and 1, respectively. Therefore, the symmetry number used for the forward reaction is 12.[44,45] The electronically excited $^2\Pi_{1/2}$ state with an excitation energy of 140 cm^{-1} was included when calculating the reactant electronic partition functions of OH. All other species are assumed to have significant population only in their ground electronic states.

Reaction rate constants were calculated at the CVT/SCT level.[13,46] A key aspect of the CVT/SCT calculations is a generalized normal-mode analysis at each point along the reaction coordinate.[13,22,47,48] The CVT level has been used rather than the canonical unified statistical[13,49] theory because only a single local maximum was found in the free energy of activation profile. The present work agrees with previous work[50] that large-curvature tunneling is negligible, so the SCT level has been used to calculate the tunneling.

2.3. Frequency Scaling. The unscaled zero-point energy (ZPE) for the CH_4 and H_2O molecules for the calculated methods is listed in Table 2 along with the experimental ZPE as inferred from spectroscopic data by Martin.[51] The ratio of the experimental anharmonic ZPE to the calculated harmonic ZPE is tabulated to show that all of the theoretical methods systematically overestimate the ZPE. The frequencies are therefore scaled to adjust for this effect. The ZPE calculated with the scaled frequencies can be found in Table 3 along with the frequency scaling factors. A database of such frequency scaling factors[25,28,35] is maintained at http://comp.chem.umn.edu/database/freq_scale.htm.

TABLE 2: Zero-Point Energies (ZPEs) for CH_4 and H_2O and Ratios of Experimental Anharmonic ZPEs to Calculated Harmonic ZPEs

	ZPE (kcal/mol)		experiment/calculated ratio ZPE (kcal/mol)	
	CH_4	H_2O	CH_4	H_2O
experiment[a]	27.71	13.24		
MCG3/3	27.99	13.43	0.9900	0.9862
MC3BB	28.57	13.69	0.9700	0.9672
MC3MPW	28.61	13.70	0.9685	0.9667
M06-2X/MG3S	28.31	13.60	0.9790	0.9736
BB1K/MG3S	28.59	13.85	0.9693	0.9559
MPW1K/MG3S	28.67	13.94	0.9664	0.9498

[a] From ref 51.

TABLE 3: Experimental and Scaled Zero-Point Energies (ZPEs) for CH_4 and H_2O and Frequency Scaling Factors

	ZPE (kcal/mol)		
	CH_4	H_2O	scaling factor
experiment	27.71	13.24	
MCG3/3	27.69	13.28	0.9893[a]
MC3BB	27.64	13.24	0.9675[b]
MC3MPW	27.66	13.24	0.9669[b]
M06-2X/MG3S	27.80	13.35	0.9820[c]
BB1K/MG3S	27.41	13.28	0.9590[d]
MPW1K/MG3S	27.47	13.36	0.9581[d]

[a] This work. [b] From ref 25. [c] From ref 29. [d] From ref 28.

A general frequency scaling factor has not been published for the MCG3/3 method. The reactants and products for the system of interest are composed entirely of C−H and O−H single bonds. Therefore, a frequency scaling factor for this level has been determined using only the CH_4 and H_2O molecules rather than the full 13 molecules in the Martin[51] compilation. A value of 0.9893 for the MCG3/3 frequency scaling factor has been determined by minimizing the root-mean-square error in ZPE for the CH_4 and H_2O molecules.

2.4. Hindered Internal Rotation. The internal rotation, or torsion, of the $-OH$ group with respect to the $-CH_3$ group during the reaction is a nearly free rotation with a very low harmonic frequency. This vibrational degree of freedom is particularly problematic for two reasons: (1) The harmonic frequency associated with this mode has numerical fluctuations along the MEP where relatively small changes in this low frequency cause a large change in the harmonic partition function, and (2) the harmonic oscillator approximation is an inadequate model for this type of motion.

The harmonic oscillator (HO) partition function[52] for each vibrational mode m is given by

$$Q_m^{\mathrm{HO}} = \frac{e^{-\beta\hbar\omega_m/2}}{1 - e^{-\beta\hbar\omega_m}} \tag{2}$$

where ω_m is the harmonic vibrational frequency of mode m. A method has been proposed[53] in which the partition function for the torsional mode (labeled by subscript tor) is estimated via

$$Q_{\mathrm{tor}} = Q_{\mathrm{tor}}^{\mathrm{HO}} \tanh\left(\frac{Q_{\mathrm{FR}}}{Q^{\mathrm{I}}}\right) \tag{3}$$

where $Q_{\mathrm{tor}}^{\mathrm{HO}}$ is given by eq 2 and Q^{I} and Q_{FR} are intended to model the partition function at intermediate temperatures and in the high-temperature, free-internal-rotator limit, respectively. The intermediate-temperature partition function, Q^{I}, is evaluated by taking the high-temperature limit of eq 2

$$Q^{\mathrm{I}} = \frac{1}{\hbar\beta\omega_{\mathrm{tor}}} \tag{4}$$

where $\hbar$ is Planck's constant divided by 2π. The free-internal-rotation partition function, Q_{FR}, is given by

$$Q_{\mathrm{FR}} = \frac{(2\pi IkT)^{1/2}}{\hbar\sigma} \tag{5}$$

where σ is the internal-rotational symmetry number, which is 3 at the transition state because there are three equivalent wells as the OH group rotates 360° with respect to the CH_3 group. I is the effective reduced moment of inertia for internal rotation.

Two methods for calculating the effective reduced moment of inertia for internal rotation are readily applied for evaluation of eq 3 along an MEP. The first is the method of Pitzer,[9,11] which is designated as the curvilinear scheme, or C-scheme. This scheme requires that the system is partitioned into two rotating subsystems and that one choose an axis of rotation, which has been chosen here as the carbon−oxygen axis. The second is a method proposed by one of us;[53] this method is designated as the rectilinear scheme, or R-scheme. This method also requires that the system is partitioned into rotating sections, but it does not require a user-supplied axis of rotation. The R-scheme calculates the angular momentum vectors of the rotating subsystems from the corresponding generalized normal-mode eigenvector, and then it places the axis of rotation through the center of mass of the system and parallel to either of the subsystem angular momentum vectors. (They are antiparallel so it does not matter which is chosen.) These two methods are equivalent for highly symmetric systems such as ethane, but they differ for systems that are off-balance. The C-scheme seems to be more accurate for large systems,[54] but it is not clear which method is more accurate for small systems, such as HO−H−CH_3.

When the torsional potential is represented by a simple cosine curve, the moment of inertia, the torsional frequency, and the barrier height, W, are related by

$$\omega_{\mathrm{tor}} = \sigma\left(\frac{W}{2I}\right)^{1/2} \tag{6}$$

Due to the difficulty in calculating reliable harmonic frequencies for a torsional mode with a very low barrier, this equation has been used to calculate the torsional frequency from the barrier height and the effective reduced moment of inertia. This has been done with the R-scheme and C-scheme, with the resulting methods labeled RW and CW,[54,55] respectively. The barrier height for internal rotation at the saddle point is determined by adjusting the dihedral angle associated with the torsion while keeping the bond formation and breakage distances fixed and all other degrees of freedom relaxed. Calculations at the MPW1K/MG3S, MC3BB, and MC3MPW levels indicate that the barrier is in the 2.5−3.5 cm^{-1} range, but even with a value of 5 cm^{-1}, the internal-rotation partition function is in the free-internal-rotation limit; therefore we use eq 5 rather than eqs 3 or 2 for all rate constant calculations in this article. In the MCG3/3 calculations, we use $W = 5$ cm^{-1} at every s.

It is not obvious how to partition the system into two groups. The hydrogen atom that is being transferred could reasonably be placed with either the $-OH$ or the $-CH_3$ group. To examine the impact of the system partitioning on the moment of inertia, the information used to calculate the torsional partition function has been listed in Tables 4 and 5. Table 4 contains results at

TABLE 4: Torsional Data Obtained Using MCG3/3 with a Barrier to Internal Rotation of 5 cm^{-1} at 225 K[a]

isotope	method	I (a.u.)	Q_{FR}	Q_{tor}^{HO}	Q^{I}	Q_{tor}
^{12}C	CW CH_3-H_2O	4607.1	1.5139	4.7679	4.7766	1.4625
	CW CH_4-OH	4564.3	1.5068	4.7456	4.7544	1.4556
	RW CH_3-H_2O	7830.6	1.9736	6.2207	6.2274	1.9081
	RW CH_4-OH	7443.0	1.9242	6.0645	6.0713	1.8601
^{13}C	CW CH_3-H_2O	4607.1	1.5139	4.7679	4.7766	1.4625
	CW CH_4-OH	4564.3	1.5068	4.7456	4.7544	1.4556
	RW CH_3-H_2O	7956.9	1.9895	6.2708	6.2774	1.9234
	RW CH_4-OH	7689.4	1.9558	6.1642	6.1710	1.9558
$^{12}C/^{13}C$	CW CH_3-H_2O	1.0000	1.0000	1.0000	1.0000	1.0000
	CW CH_4-OH	1.0000	1.0000	1.0000	1.0000	1.0000
	RW CH_3-H_2O	0.9841	0.9920	0.9920	0.9920	0.9920
	RW CH_4-OH	0.9680	0.9838	0.9838	0.9838	0.9511

[a] ω_{tor} is calculated by eq 6 with $W = 5$ cm^{-1}.

TABLE 5: Torsional Data Obtained Using MCG3/3 with a Barrier to Internal Rotation of 5 cm^{-1} at 300 K[a]

isotope	method	I (a.u.)	Q_{FR}	Q_{tor}^{HO}	Q^{I}	Q_{tor}
^{12}C	CW CH_3-H_2O	4607.1	1.7481	6.3623	6.3689	1.7037
	CW CH_4-OH	4564.3	1.7399	6.3326	6.3392	1.6957
	RW CH_3-H_2O	7830.6	2.2790	8.2981	8.3032	2.2221
	RW CH_4-OH	7443.0	2.2219	8.0899	8.0951	2.1663
^{13}C	CW CH_3-H_2O	4607.1	1.7481	6.3623	6.3689	1.7037
	CW CH_4-OH	4564.3	1.7399	6.3326	6.3392	1.6957
	RW CH_3-H_2O	7956.9	2.2973	8.3649	8.3698	2.2399
	RW CH_4-OH	7689.4	2.2583	8.2229	8.2280	2.2583
$^{12}C/^{13}C$	CW CH_3-H_2O	1.0000	1.0000	1.0000	1.0000	1.0000
	CW CH_4-OH	1.0000	1.0000	1.0000	1.0000	1.0000
	RW CH_3-H_2O	0.9841	0.9920	0.9920	0.9920	0.9921
	RW CH_4-OH	0.9680	0.9839	0.9838	0.9838	0.9593

[a] ω_{tor} is calculated by eq 6 with $W = 5$ cm^{-1}

thesaddle point based on the RW- and CW-schemes with both choices of partitioning at 225 K, and Table 5 does the same at 300 K.

Certain features are apparent for all of the methods involved in these tabulations. The first is that the system is close to the free-rotator limit, and the harmonic oscillator approximation is inadequate. The second is that the torsional partition function is less than the free rotator partition function. The hyperbolic tangent in eq 3 was chosen to yield a smooth transition between the harmonic oscillator partition function and the free rotator partition function, but for this system the functional form passed the free rotator partition function. Therefore, for the remainder of the calculations in this article, the partition function for the torsional mode will be represented by the free-rotator partition function calculated using eq 5.

The tables also show that the C-scheme does not predict a significant difference between the ^{12}C and the ^{13}C cases. This result is not obvious without doing the calculations because (contrary to an incorrect statement in ref 7) the C-scheme is not independent of a mass change in an atom on the rotational axis; for example, the calculated moments of inertia for H_2O_2 and $H_2{}^{18}O_2$ using the C-scheme and the oxygen−oxygen axis are 2754.9 $m_e a_0^2$ and 2774.8 $m_e a_0^2$, respectively.[54] The moments of inertia for the ^{12}C and ^{13}C systems are not exactly the same, but they are equivalent to five significant digits. Accordingly, the free-rotator partition functions are also equivalent to five significant digits.

Finally, it should be noted that the choice of the group in which the transferring hydrogen atom is placed has a significant effect on the partition function, and the effect is larger for the R-scheme. However, it is not clear which choice is best. The discussion of the torsional mode will be revisited in the discussion of the kinetic isotope effect in section 3.

TABLE 6: Stretches, Bends, and Torsions for the Nonredundant Internal Coordinates

stretches	bends	torsions
1−5	5−1−4	5−1−3−2
1−4	4−1−6	1−3−2−7
1−6	6−1−5	
1−3	4−1−3	
3−2	6−1−3	
2−7	1−3−2	
	3−2−7	

TABLE 7: Additional Stretches, Bends, and Torsions for the Redundant Internal Coordinates[a]

stretches	bends	torsions
1−2	5−1−2	5−1−2−7
	1−2−7	
	4−1−2	
	6−1−2	

[a] In addition to those in Table 6.

2.5. Coordinate Systems. The vibrational frequencies at a stationary point are independent of the coordinate system if a complete set of coordinates is used. However, this is not the case for frequencies of a generalized transition state on the MEP. Three coordinate systems have been tested in this article. The first is the set of $3N$ mass-scaled Cartesian coordinates, where N is the number of atoms (which is 7 for OH + CH_4). Cartesian coordinates are also called rectilinear coordinates, but it is more physical to use internal coordinates such as bond stretches, bond angles, and torsional angles, which are nonlinear functions of Cartesian coordinates and hence are called curvilinear. The second coordinate system is a set of $3N - 6$ nonredundant curvilinear internal coordinates. The set of stretches, bends, and torsions used for the nonredundant curvilinear internal coordinates is listed in Table 6. The third coordinate system considered is a set of $3N$ redundant internal coordinates.[56] The additional coordinates are specified in Table 7. This set includes all of the coordinates in the nonredundant set along with several coordinates that bypass the transferring hydrogen atom, such as the carbon−oxygen distance. Of course, the results would be independent of the coordinate system if no approximation were made, but in practice one makes several approximations, the most important of which is the truncation of the expansion of the potential energy at quadratic terms, except for torsional anharmonicity. As a general rule redundant internal coordinates are more physical than nonredundant ones, and either set of curvilinear coordinates is more physical than Cartesian coordinates, which are used by many workers simply because they are convenient. It should be noted that the choice of coordinate system changes the frequencies because it changes the definition of the generalized transition state dividing surface in coordinate space.[47,57] (The value s_*^{CVT} of the variables determines where the generalized transition state intersects the MEP, but the shape of the generalized transition state off the MEP is determined by the coordinate system.)

The frequencies obtained at the MCG3/3 level for the mass-scaled Cartesian coordinate system, the nonredundant internal coordinate system, and redundant internal coordinates are plotted in Figures 2, 3, and 4, respectively. The mass-scaled Cartesian coordinate system is the worst, which is expected because it is the least natural set of coordinates for defining a generalized transition state dividing surfaces. This coordinate system causes multiple imaginary frequencies (plotted as negative numbers) to occur on both sides of the saddle. The most serious deficiency of this calculation is not simply that some frequencies become imaginary but rather is how sharply the low frequencies decrease

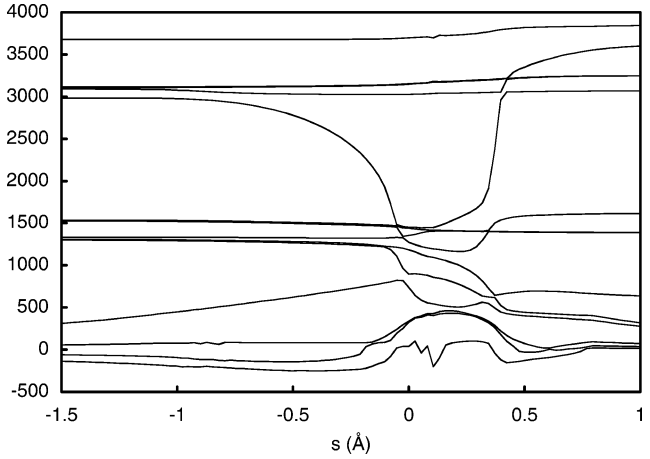

Figure 2. MCG3/3 frequencies in wave numbers (cm^{-1}) on the MEP calculated with Cartesian coordinates.

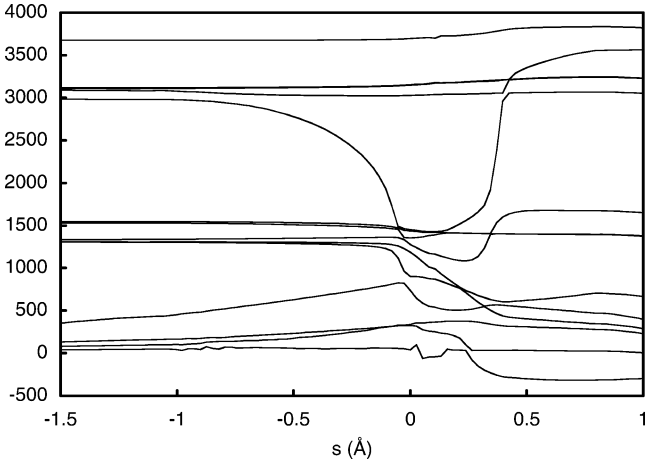

Figure 3. MCG3/3 frequencies in wave numbers (cm^{-1}) on the MEP calculated with nonredundant internal coordinates.

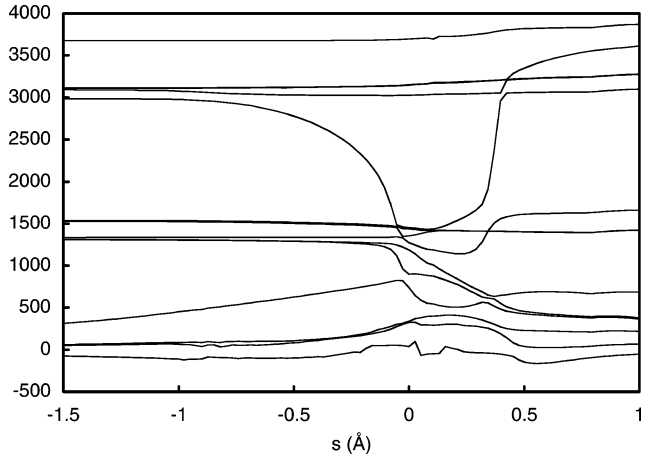

Figure 4. MCG3/3 frequencies in wave numbers (cm^{-1}) on the MEP calculated with redundant internal coordinates.

as one leaves the saddle point. This has a dramatic effect on the location of the dividing surface when calculating a CVT rate constant. Table 8 lists the location of the dividing surface and the magnitude of the variational effect (k^{TST}/k^{CVT} where k denotes a rate constant and TST denotes conventional transition state theory). The internal coordinate systems predict that the dynamical bottleneck occurs in the region of $s = -0.05$ Å. Table 9 shows large differences between the three sets of calculated frequencies at $s = -0.1$ Å. The variance in frequencies is the cause of the large difference in variational effects for the various coordinate systems.

TABLE 8: Location of the Variational Dividing Surface at 300 K, TST and CVT Rate Constants (in cm^3 $molecule^{-1}$ s^{-1}) for the Three Coordinate Systems, and the TST to CVT Ratios Calculated Using MCG3/3[a]

coordinates	s_*^{CVT} (Å)	TST ($s = 0$)	CVT ($s = s_*^{CVT}$)	TST/CVT
redundant	−0.0620	4.14×10^{-15}	1.53×10^{-15}	2.70
nonredundant	−0.1258	4.14×10^{-15}	6.25×10^{-16}	6.62
Cartesian	0.0106	4.14×10^{-15}	4.03×10^{-15}	1.03

[a] The torsional treatment is RW(CH_3-H_2O).

TABLE 9: Calculated Frequencies in cm^{-1} of the Generalized Transition State at $s = -0.106$ Å (−0.2 bohr) as Obtained with MCG3/3 RW(CH_3-H_2O)

mass-scaled Cartesian coordinates	nonredundant internal coordinates	redundant internal coordinates
3681	3681	3681
3135	3135	3135
3131	3131	3131
3022	3021	3021
1929	1930	1930
1475	1495	1481
1460	1469	1465
1322	1358	1333
1223	1280	1263
1215	1226	1222
789	792	791
153	307	254
87	303	221
141i	57	50

The two sets of internal coordinates yield similar results that are markedly different from the mass-scaled Cartesian results, and they are also qualitatively and quantitatively different from each other. The differences are illustrated in Table 9 for the reactant side of the saddle point but are also apparent on the product side of the MEP, where one of the frequencies calculated with the nonredundant internal coordinates takes a sharp dive around $s = 0.3$ Å and quickly reaches 300i cm^{-1}. The second lowest frequency approaches zero much more quickly in nonredundant internal coordinates than in redundant internal coordinates, and it becomes imaginary by $s = 1.0$ Å in nonredundant internal coordinates.

The redundant set of internal coordinates is not without problems. The frequency associated with the torsional mode fluctuates in an erratic manner and is usually imaginary. However, the torsional mode is replaced by a free internal rotator when calculating the partition function, and the frequency remains smooth and real in the important region where the bottleneck occurs, -0.3 Å $< s < 0$ Å.

One possibility for optimizing frequencies along the MEP is the RODS algorithm,[58] where RODS stands for "reorientation of the dividing surface." The RODS algorithm reorients the dividing surface to maximize the generalized free energy of activation such that the generalized transition state dividing surface need no longer be normal to the MEP; this may be required if the calculated MEP is not a good representation of the true MEP. The RODS algorithm was employed for each of the three sets of coordinate systems, and the results are given in the Supporting Information. The resulting frequencies are erratic, although the erratic frequencies could probably be improved by further adjustment of numerical parameters; however, we concluded that RODS need not be used here.

Both sets of internal coordinates yield smooth zero-point energies along the MEP. The ground-state vibrationally adiabatic

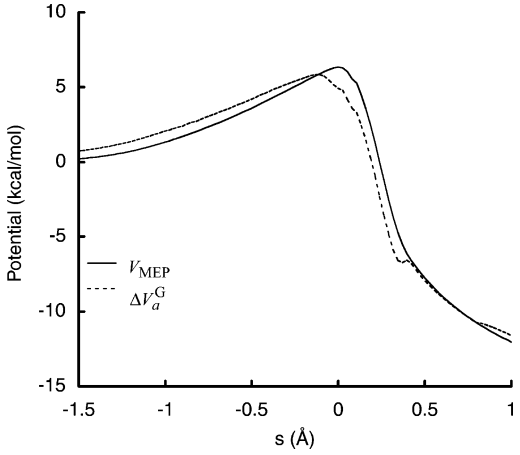

Figure 5. MCG3/3 $V_{MEP}(s)$ and $\Delta V_a^G(s)$ calculated with nonredundant internal coordinates.

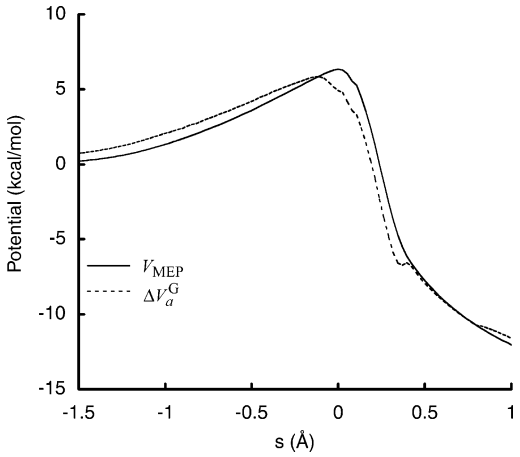

Figure 6. MCG3/3 $V_{MEP}(s)$ and $\Delta V_a^G(s)$ calculated with redundant internal coordinates.

potential, $V_a^G(s)$, is defined as the sum of the potential energy along the MEP, $V_{MEP}(s)$, plus the zero-point energy of the bound vibrational modes; the relative vibrationally adiabatic ground-state potential, $\Delta V_a^G(s)$, is defined for bimolecular reactions as $V_a^G(s)$ minus the zero-point energy for reactants.[13] A single maximum occurs in the ground-state adiabatic potential curve, $V_a^G(s)$, near the transition state, as opposed to the double peak found by Espinosa-García and Corchado;[59] this difference probably arises from the difference in potential energy surfaces. The $V_{MEP}(s)$ and $\Delta V_a^G(s)$ potential energy curves for the MCG3/3 potential energy surface have been plotted for nonredundant internal coordinates and redundant internal coordinates in Figures 5 and 6, respectively.

3. Results

3.1. Forward Rate Constants for the OH + CH_4 → H_2O + CH_3 Reaction. The forward rate constants for the MCG3/3, MC3BB, MC3MPW, M06-2X/MG3S, BB1K/MG3S, and MPW1K/MG3S levels of theory have been calculated and compared to the published three-parameter fits of Baulch et al.[60] (valid from 240 to 2500 K) and Demore et al.[61] (valid from 200 to 420 K, although superseded by the more recent Baulch et al. evaluation for $T \geq 240$ K). This rate constant comparison has been carried out using the nonredundant and redundant internal coordinates discussed in section 2; the R-scheme with CH_3-H_2O partitioning has been used because it yields the largest free-internal-rotator partition function and therefore can

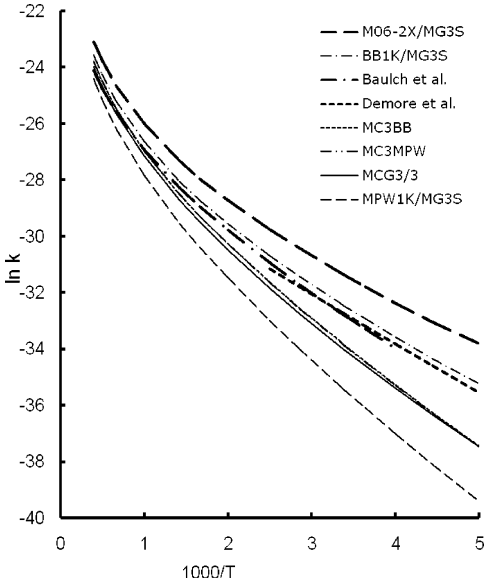

Figure 7. Forward rate constants calculated with nonredundant internal coordinates with the RW(CH_3-H_2O) torsional treatment.

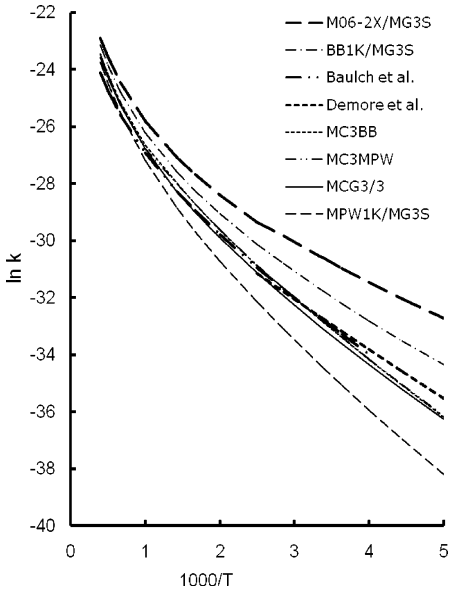

Figure 8. Forward rate constants calculated with redundant internal coordinates with the RW(CH_3-H_2O) torsional treatment.

be considered to yield an upper bound on the contribution of the torsional mode. The results of these calculations are in Figures 7 and 8 and are tabulated in the Supporting Information.

Even using the torsional method that maximizes the rate constant, the calculated rate constants for the higher-level multilevel methods are too low compared to the recommended values in the 200−300 K range. The use of the C-scheme with the CH_4-OH partitioning lowers the rate constant about 25% relative to the values given. The use of redundant internal coordinates yields better agreement of the forward rate constants with the recommended results than the use of nonredundant internal coordinates. As compared to the 2005 evaluation,[60] nonredundant-coordinate MCG3/3 calculations are too high by a factor that decreases from a factor of 4.1 at 250 K to a factor of 1.3 at 1000 K, and this calculation agrees with experiment within 14% for 1500−2500 K. With redundant internal coordinates, the calculations are too low by factor decreasing from 1.4 at 250 K to 1.04 at 700 K and too high by a factor that increases from 1.1 at 1000 K to 1.7 at 2500 K. One can hardly

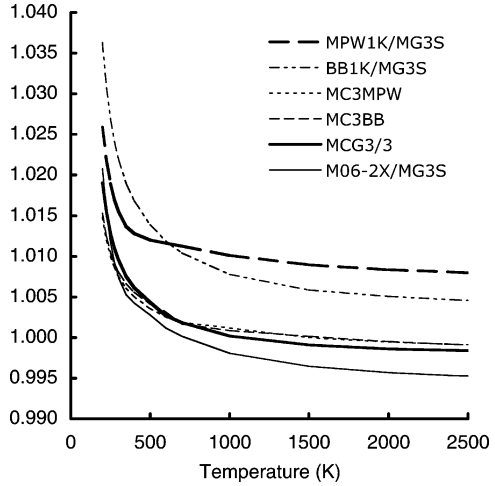

Figure 9. $^{12}C/^{13}C$ kinetic isotope effect with MCG3/3 and other electronic structure levels by using nonredundant internal coordinates and the RW(CH_3-H_2O) torsonal treatment.

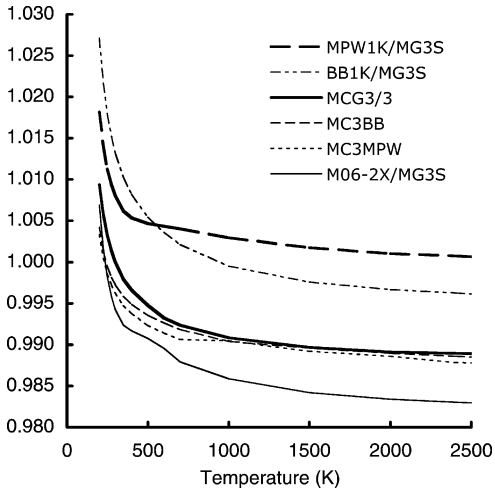

Figure 10. $^{12}C/^{13}C$ kinetic isotope effect with MCG3/3 and other electronic structure levels by using nonredundant internal coordinates and the RW(CH_4-OH) torsonal treatment.

ask for better agreement of theory and experiment over such a wide temperature range.

3.2. $^{12}C/^{13}C$ Kinetic Isotope Effect. The $^{12}C/^{13}C$ kinetic isotope effect for the $OH + CH_4 \rightarrow H_2O + CH_3$ reaction has been measured experimentally at 296 K. The published results are 1.0039 by Cantrell et al.[3] and 1.0054 by Saueressig et al.[4] This effect also has been studied theoretically[7,8,59] in recent years, including previous work[7] by the present authors.

The $^{12}C/^{13}C$ kinetic isotope effect has been calculated in the present work for both sets of internal coordinates, each with the four types of treatment for the torsional mode. The four torsional treatments considered are the RW-scheme with CH_3-H_2O partitioning, designated RW(CH_3-H_2O); the RW-scheme with CH_4-OH partitioning, designated RW(CH_4-OH); the CW-scheme with CH_3-H_2O partitioning, designated CW(CH_3-H_2O); and the CW-scheme with CH_4-OH partitioning, designated CW(CH_4-OH). The results calculated using nonredundant internal coordinates are found in Figures 9−12. The results calculated using redundant internal coordinates are found in Figures 13−16. The data from which Figures 9−16 have been constructed have been tabulated in the Supporting Information.

3.2.1. MCG3/3 Results. MCG3/3 is the highest level of theory that has been applied to the $^{12}C/^{13}C$ kinetic isotope effect. The KIEs calculated with the MCG3/3 level of theory for the RW-

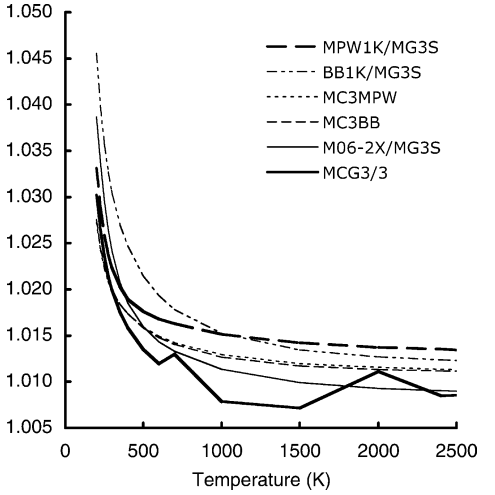

Figure 11. $^{12}C/^{13}C$ kinetic isotope effect with MCG3/3 and other electronic structure levels by using nonredundant internal coordinates and the CW(CH_3-H_2O) torsonal treatment.

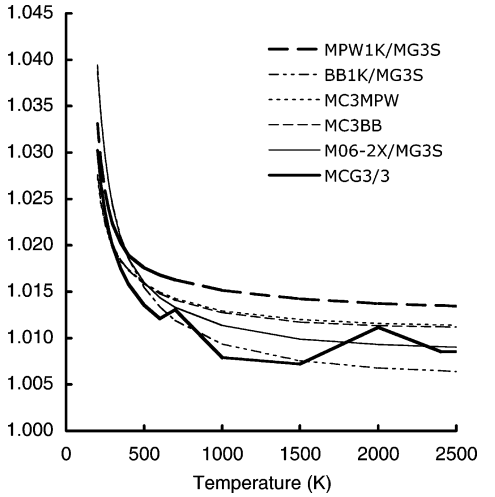

Figure 12. $^{12}C/^{13}C$ kinetic isotope effect with MCG3/3 and other electronic structure levels by using nonredundant internal coordinates and the CW(CH_4-OH) torsonal treatment.

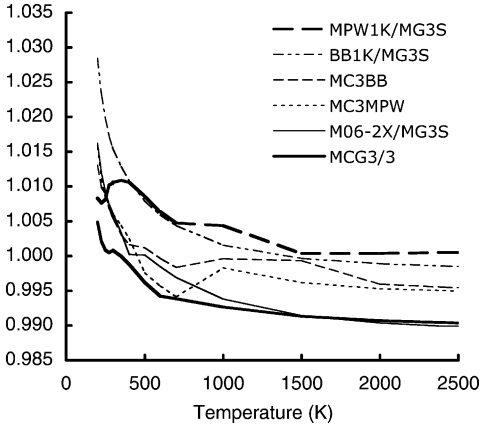

Figure 13. $^{12}C/^{13}C$ kinetic isotope effect with MCG3/3 and other electronic structure levels by using redundant internal coordinates and the RW(CH_3-H_2O) torsonal treatment.

(CH_3-H_2O), RW(CH_4-OH), and CW(CH_3-H_2O) torsional methods using both nonredundant and redundant internal coordinates have been plotted in Figure 17 and tabulated in the Supporting Information. The results based on CW(CH_4-OH) torsional treatment have not been included since the KIEs with this torsional method are virtually identical to those obtained

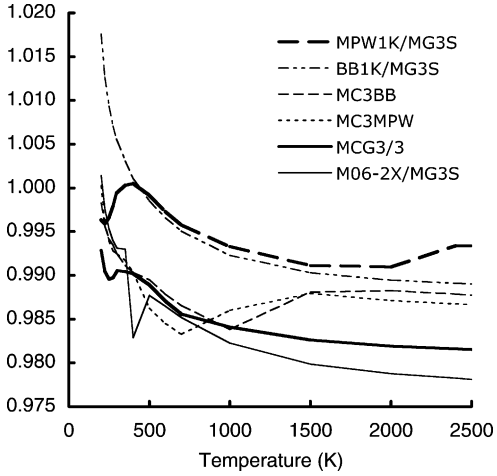

Figure 14. $^{12}C/^{13}C$ kinetic isotope effect with MCG3/3 and redundant internal coordinates and the RW(CH_4-OH) torsonal treatment.

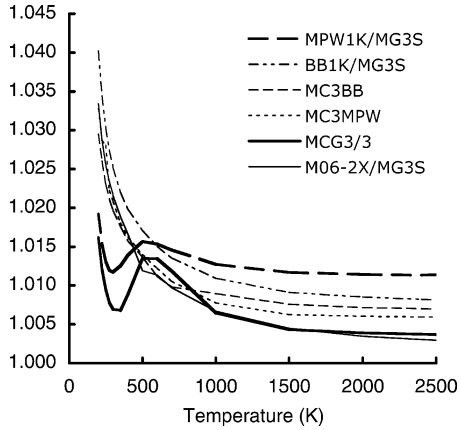

Figure 15. $^{12}C/^{13}C$ kinetic isotope effect with MCG3/3 and redundant internal coordinates and the CW(CH_3-H_2O) torsonal treatment.

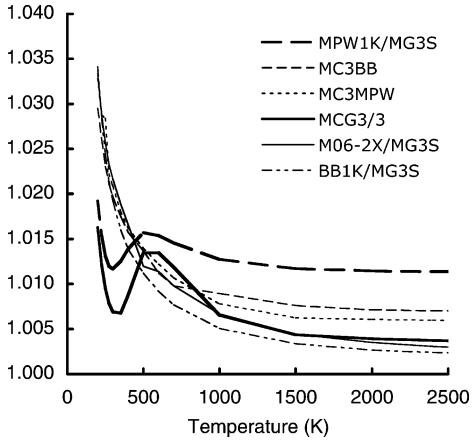

Figure 16. $^{12}C/^{13}C$ kinetic isotope effect with MCG3/3 and redundant internal coordinates and the CW(CH_4-OH) torsonal treatment.

with the CW(CH_3-H_2O) torsional method. Figure 17 clearly demonstrates the dramatic effect that a change in torsional method or coordinate system can have on the calculated $^{12}C/^{13}C$ kinetic isotope effect.

The tables and figures show that the KIEs calculated with redundant internal coordinates have smaller values and are more erratic than the KIEs calculated with nonredundant internal coordinates. It is clear that the redundant internal coordinate calculations suffer from a lack of precision; however, the smooth curves from the nonredundant internal coordinate calculations may be systematically incorrect. Previous work[56] has shown

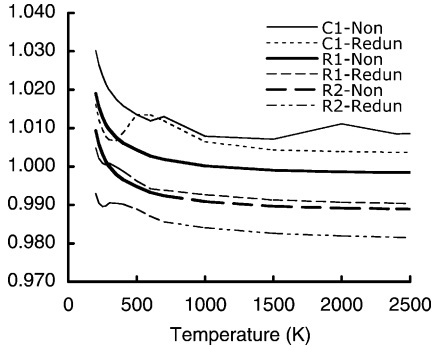

Figure 17. $^{12}C/^{13}C$ kinetic isotope effect with the MCG3/3 level of theory. The RW(CH_3-H_2O), RW(CH_4-OH), and CW(CH_3-H_2O) torsonal methods with nonredundant internal coordinates are labeled R1-Non, R2-Non, and C1-Non, respectively. The RW(CH_3-H_2O), RW(CH_4-OH), and CW(CH_3-H_2O) torsonal methods with redundant internal coordinates are labeled R1-Redun, R2-Redun, and C1-Redun, respectively.

TABLE 10: $^{12}C/^{13}C$ Coordinate System Correction and the Corrected Kinetic Isotope Effects as Obtained with the MCG3/3 Level of Theory[a]

T (K)	correction	R1-Corr	R2-Corr	C1-Corr	MCG3/3 (corrected)	MCG3/3 (H&H)
200	0.0149	1.0041	0.9945	1.0153	1.0081	1.0097
225	0.0144	1.0011	0.9914	1.0121	1.0049	1.0066
250	0.0133	0.9996	0.9900	1.0104	1.0034	1.0050
275	0.0119	0.9990	0.9894	1.0096	1.0027	1.0043
296	0.0106	0.9992	0.9895	1.0094	1.0028	1.0043
300	0.0104	0.9992	0.9896	1.0095	1.0028	1.0043
350	0.0086	0.9989	0.9893	1.0089	1.0024	1.0039
400	0.0069	0.9993	0.9897	1.0089	1.0026	1.0041
500	0.0047	0.9997	0.9901	1.0088	1.0029	1.0043
600	0.0044	0.9983	0.9888	1.0075	1.0015	1.0029
700	0.0053	0.9965	0.9871	1.0077	1.0004	1.0021
1000	0.0052	0.9950	0.9856	1.0026	0.9977	0.9988
1500	0.0059	0.9932	0.9838	1.0013	0.9960	0.9972
2000	0.0074	0.9912	0.9817	1.0037	0.9955	0.9974
2400	0.0067	0.9917	0.9822	1.0018	0.9952	0.9967
2500	0.0068	0.9916	0.9822	1.0018	0.9952	0.9967

[a] The R1-Corr, R2-Corr, and C1-Corr schemes are defined in eqs 8, 9, and 10, respectively. MCG3/3(corrected) is defined in eq 11. MCG3/3(H&H) is defined in the last paragraph of subsection 3.2.1.

the merits of redundant internal coordinates; however, the choice of coordinates as those that bypass the transferring atom (as used here) has not been well-studied, and the appropriateness is unknown. As noted in subsection 3.1, the use of redundant internal coordinates for the forward rate constants yields better agreement with the recommended results than the use of nonredundant internal coordinates.

The differences between the calculated KIEs using the same torsional method but with the two different internal coordinate systems were calculated. This was done for each torsional method found in Figure 17, and the average of these differences for each temperature is defined as the coordinate correction value and is listed in Table 10

$$\text{Correction}(T) = \frac{1}{3}[\text{KIE(R1-Non},T) - \text{KIE(R1-Redun},T) + \text{KIE(R2-Non},T) - \text{KIE(R2-Redun},T) + \text{KIE(C1-Non},T) - \text{KIE(C1-Redun},T)] \quad (7)$$

where the RW(CH_3-H_2O), RW(CH_4-OH), and CW(CH_3-H_2O) torsional methods with nonredundant internal coordinates are labeled R1-Non, R2-Non, and C1-Non, respectively, and the RW(CH_3-H_2O), RW(CH_4-OH), and CW(CH_3-H_2O)

TABLE 11: $^{12}C/^{13}C$ Kinetic Isotope Effect Ratios for the MCG3/3 Level of Theory

T (K)	R1-Non/ C1-Non	R2-Non/ C1-Non	R1-Redun/ C1-Redun	R2-Redun/ C1-Redun
200	0.989	0.980	0.989	0.977
225	0.989	0.980	0.990	0.979
250	0.989	0.980	0.991	0.980
275	0.990	0.980	0.993	0.982
296	0.990	0.980	0.994	0.983
300	0.990	0.980	0.994	0.984
350	0.990	0.981	0.993	0.984
400	0.990	0.981	0.990	0.982
500	0.991	0.982	0.983	0.976
600	0.991	0.982	0.981	0.974
700	0.989	0.980	0.982	0.974
1000	0.992	0.983	0.986	0.978
1500	0.992	0.983	0.987	0.978
2000	0.988	0.978	0.987	0.978
2400	0.990	0.981	0.987	0.978
2500	0.990	0.981	0.987	0.978

torsional methods with redundant internal coordinates are labeled R1-Redun, R2-Redun, and C1-Redun, respectively. The coordinate correction has been subtracted from the smooth KIEs calculated with nonredundant internal coordinates to define the R1-Corr, R2-Corr, and C1-Corr adjusted estimates of the KIEs

$$\mathrm{KIE(R1\text{-}Corr},T) = \mathrm{KIE(R1\text{-}Non},T) - \mathrm{Correction}(T) \quad (8)$$

$$\mathrm{KIE(R2\text{-}Corr},T) = \mathrm{KIE(R2\text{-}Non},T) - \mathrm{Correction}(T) \quad (9)$$

$$\mathrm{KIE(C1\text{-}Corr},T) = \mathrm{KIE(C1\text{-}Non},T) - \mathrm{Correction}(T) \quad (10)$$

The resulting corrected KIEs are also tabulated in Table 10.

The experimentally determined KIE lies between the R1-Corr and the C1-Corr values. It is valuable to examine the ratios of the KIEs with different torsional methods and compare them to the KIE contributions of the torsional mode that are listed in Tables 4 and 5. The KIE ratios have been tabulated in Table 11. These overall KIE values are heavily correlated with the KIE contributions of the torsional mode. The KIE ratio for the R(CH_3-H_2O) and C(CH_3-H_2O) torsional method alone is 0.992, and the KIE ratio for the complete system using the same torsional methods is about 0.990 across the temperature range. The KIE ratio for the R(CH_4-OH) and C(CH_3-H_2O) torsional method alone is 0.984, and the KIE ratio for the complete system using the same torsional methods is close to 0.980 across the whole temperature range.

The KIE for the torsional mode is seen above to be of critical importance in determining the KIE. Insight into this factor can be obtained from the normal-mode analysis at the saddle point. The frequencies associated with the torsional mode at the saddle point are 38.44 and 38.24 cm^{-1} for the ^{12}C and ^{13}C systems, respectively. When the torsional potential is represented by a simple cosine curve, which is appropriate for this system, eq 6 shows that the frequency and the moment of inertia are related. All other variables in eq 6 are unchanged between the ^{12}C and the ^{13}C systems; therefore, the ratio of the frequencies can be used to yield a ratio of 0.9896 for the moment of inertia. Equation 5 can then be used to determine the ratio of the ^{12}C and ^{13}C free-rotor partition functions, yielding 0.9948.

If the resulting KIE for the torsional mode of 0.9948 is correct, then this indicates that the correct value for the KIE of the forward reaction lies between the results obtained using the RW(CH_3-H_2O) and CW(CH_3-H_2O) torsional methods. Indeed, the experimentally determined KIE does lie between the values

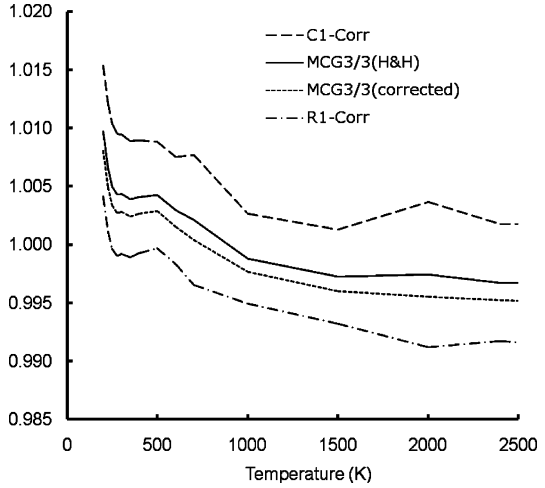

Figure 18. $^{12}C/^{13}C$ kinetic isotope effect with R1-Corr, C1-Corr, MCG3/3(corrected), and MCG3/3(H&H).

obtained using the RW(CH_3-H_2O) and CW(CH_3-H_2O) torsional methods with the coordinate-corrected MCG3/3 level of theory. A quantitative value for a correction to the torsional mode can be determined using the free-rotor partition functions. The KIE for the torsional mode of 0.9948, as determined using the frequency from the normal-mode analysis to determine the moment of inertia, falls 35% of the way between the KIE for the torsional modes using the RW(CH_3-H_2O) and CW(CH_3-H_2O) torsional methods. Therefore, the coordinate and torsional corrected MCG3/3 KIE is defined as

$$\mathrm{MCG3/3(corrected)} = \mathrm{KIE(R1\text{-}Corr)} + 0.35[\mathrm{KIE(C1\text{-}Corr)} - \mathrm{KIE(R1\text{-}Corr)}] \quad (11)$$

where KIE(R1-Corr) is the coordinate-corrected KIE using the RW(CH_3-H_2O) torsional method and KIE(C1-Corr) is the coordinate-corrected KIE using the CW(CH_3-H_2O) torsional method. The KIEs for MCG3/3(corrected) are listed in Table 10. The KIEs for R1-Corr, C1-Corr, and MCG3/3(corrected) have been plotted in Figure 18.

The values calculated using the MCG3/3(corrected) method are very close to the experimental values (1.003 vs 1.004−1.005 at 296 K). The fact that the calculated values are slightly too low indicates that the MCG3/3(corrected) method should contain a greater contribution from the C-scheme than it currently does. Previous work[54] gives support to this conclusion. It has been determined that the C-scheme yields better effective reduced moments of inertia for a one-dimensional internal rotation, especially for off-balance molecules. However, the C-scheme does not itself determine the correct axis of rotation; rather, it requires a user-defined axis, and it compensates for changes in the center of mass resulting from rotation about the user-defined axis. (The correct torsional motion does not move the center of mass of the system.) The C-scheme yields very reasonable effective reduced moments of inertia; however, the lack of a dynamical criterion for determining an appropriate axis of rotation is likely why the C-scheme does not correctly predict the KIE and a why a mix of R-scheme and C-scheme KIEs is required to reproduce the experimental results.

The MCG3/3 corrected half and half method, abbreviated MCG3/3(H&H), has been adjusted to reproduce the available experimental measurements, yielding a KIE of 1.0043 at 296 K. MCG3/3(H&H) is defined as the average of the KIE(R1-Corr) and KIE(C1-Corr), which is equivalent to replacing 0.35 with 0.50 in eq 11. The rate constants for the MCG3/3(H&H) method have been listed in Table 10 and plotted in Figure 18.

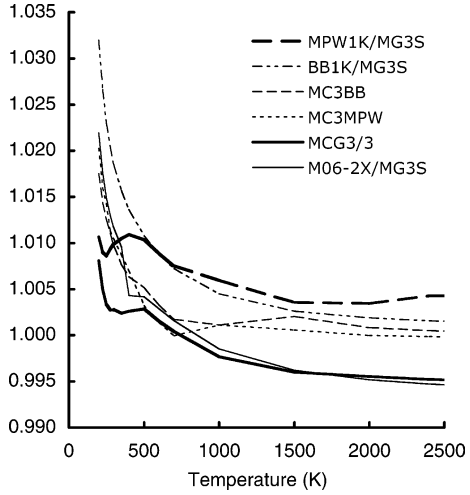

Figure 19. $^{12}C/^{13}C$ kinetic isotope effect using coordinate and torsional corrected methods.

3.2.2. Results for Other Levels of Theory. The values for the KIEs calculated using the coordinate and torsional corrected method for each level of theory have been plotted in Figure 19 and tabulated in the Supporting Information. The coordinate and torsional corrections were calculated in the same manner as eqs 7−11, where the individual terms were calculated for each level of theory. The coordinate and torsional corrected method yields reasonable KIE values; however, the other levels of theory yield systematically higher values than the MCG3/3. This is most likely the result of a less accurate PES than the MCG3/3 PES, resulting in a less accurate MEP and less accurate frequencies, which have a direct impact on the CVT rate calculated using eq 1 as well as an impact on the SCT tunneling factor.

The MCG3/3 level of theory requires more C-scheme character than the other levels of theory to reproduce the experimental results. One particularly dangerous feature of the R-scheme is its ability to significantly alter the calculated rate constants, which can result in fortuitous cancellation of error. As discussed in subsection 3.2.1, previous research indicates that the C-scheme yields better moments of inertia, so it is unlikely that torsional mode requires predominately R-scheme character. The MCG3/3 level of electronic structure theory is vastly superior[62] to any other level of the theory that has been used to study the $^{12}C/^{13}C$ kinetic isotope effect, including the other levels of theory used in the present work. Therefore, the MCG3/3 values are the most reliable results at the present time.

3.2.3. Temperature Dependence of the KIE. The calculated KIE depends on temperature, weakly at high temperatures but more so at lower temperatures. In the 200−300 K temperature range, the KIE decreases as little as 5 ppt for the MCG3/3(corrected) level of theory and as much as 13 ppt for the BB1K/MG3S(corrected) level of theory. The MPW1K/MG3S(corrected) level of theory shows a temperature dependence at high temperatures but behaves strangely at lower temperatures due to precision problems associated with nonredundant internal coordinates. The rate constants calculated at the MPW1K/MG3S level of theory show a clear temperature dependence when calculated with nonredundant internal coordinates.

The low-temperature range where the KIE is changing rapidly is the most important one for atmospheric models, yet a temperature dependence of the KIE has not yet been experimentally determined. Experimental measurements of the temperature dependence for the $^{12}C/^{13}C$ kinetic isotope effect would greatly aid in the determination of the validity of the theories studied here. However, in the absence of experiment, theory can contribute the most reliable values to be used in atmospheric climate models, and we propose that the MCG3/3(H&H) results for the $^{12}C/^{13}C$ kinetic isotope effect should used in climate models.

TABLE 12: First Factorization of the $^{12}C/^{13}C$ Kinetic Isotope Effect at 296 K

contribution[a]	CW(CH_3-H_2O)	RW(CH_3-H_2O)
η_{vib}	0.980	0.973
η_{rot}	0.971	0.971
η_{trans}	1.047	1.047
η_{pot}	1.003	1.000
η_{CRCM}	1.008	1.013
CVT/SCT KIE[b]	1.007	1.001
ICVT/SCT KIE[c]	1.007	0.996

[a] Each η denotes a factor in the MCG3/3 KIE. The factorization analyses in this table and Table 13 are based on redundant internal coordinates. [b] Product of the above factors, which equals the CVT/SCT KIE. [c] Kinetic isotope effect by improved canonical variational transition state theory with the SCT transmission coefficient.

3.2.4. Comparison to Cl + CH_4. Another reaction whose $^{12}C/^{13}C$ KIE is very important for the understanding what the isotopic composition of atmospheric methane tells us about the inferences that may be drawn from trace gas analysis of sampled air masses is the reaction of chlorine atoms with methane.[60] The $^{12}C/^{13}C$ KIE for this reaction has been measured to be 1.06 at room temperature.[60] Because the critical torsion that complicates the present work does not appear in the Cl + CH_4 reaction, its temperature dependence is easier to model.

3.2.5. Contributions to KIEs. To gain more insight into how each kind of degree of freedom, in particular vibrations (vib), rotations (rot), translations (trans), and the reaction coordinate, contributes to the $^{12}C/^{13}C$ KIE, we performed a factorization analysis[63] for this KIE at 296 K. The contribution of the reaction coordinate is further factored into a part from the potential energy (pot) and a part from coupled reaction-coordinate motion (which will be labeled CRCM). The factors are listed in Table 12, which shows that the contributions from vibrations and rotations to the KIE are less than unity, whereas the contributions from translation and CRCM are greater than unity.

The CRCM factor is the difference between the CVT/SCT result and the CVT result. This has three contributions: classical reflection, nonclassical reflection, and nonclassical tunneling. Tunneling is usually the most important of these contributions (that is, the factor deviating the most from unity), and often one just labels the CRCM factor as tunneling (η_{tun} instead of η_{CRCM}), but for heavy-atom kinetic isotope effects we need to pay attention even to factors that are close to unity because the KIE itself is so close to unity. The classical reflection is accounted for by the classical adiabatic ground-state transmission coefficient, that is, by the $\kappa^{CVT/CAG}$ transmission coefficient,[13,64] which corresponds to classical reflection by the part of $V_a^G(s)$ that is higher than $V_a^G(s_*^{CVT})$, where s_*^{CVT} is the location of the maximum of the generalized free energy of activation at the temperature under consideration. (Thus, if the maximum of $V_a^G(s)$ were at s_*^{CVT}, then the CVT/CAG factor would be unity.) The CVT/CAG factors at 296 K for redundant internal coordinates and the CH_3-H_2O partition are 0.9796 (CW, ^{12}C), 0.9796 (CW, ^{13}C), 0.9249 (RW, ^{12}C), and 0.9202 (RW, ^{13}C). We should keep in mind that a change of 0.001 kcal/mol in the interpolated maximum value of $V_a^G(s)$ makes a change of 2 ppt in the calculated rate constant at 296 K, and these CVT/CAG factors are uncertain by at least that amount. The nonclassical contributions to the CRCM factor are 3.439 (CW or RW, ^{12}C)

TABLE 13: Second Factorization of the $^{12}C/^{13}C$ Kinetic Isotope Effect at 296 K

contribution	CW(CH_3-H_2O)	RW(CH_3-H_2O)
ZPE[a]	0.988	0.988
finite-temperature torsion	1.000	0.987
CRCM[b]	1.008	1.013
all other	1.011	1.013
KIE[c]	1.007	1.001

[a] Zero-point energy at the canonical variational transition state. [b] Factor from coupled reaction-coordinate motion. [c] Product of the above factors, which equals the CVT/SCT KIE.

and 3.414 (CW or RW, ^{13}C). One way to estimate the reliability of the calculations is to redo them with improved canonical variational theory (ICVT) because ICVT involves a more consistent treatment of the threshold energies and does not require a CAG factor. We did this for the two cases in Table 12. For the RW case, the ICVT/SCT rates agree with the CVT/SCT rates to 7.5% for ^{12}C and to 8.0% for ^{13}C. This 5 ppt difference lowers the predicted KIE by 5 ppt, as shown in Table 12. For the CW case, however, the predicted KIE does not change.

Table 12 is not the only way to factorize the KIE. One can, for example, also factorize it as due to zero-point energy, finite-temperature effect of the torsion, coupled reaction-coordinate motion, and all other factors. This factorization is given in Table 13 for the CW(CH_3-H_2O) and RW(CH_3-H_2O) torsional treatments with redundant internal coordinates, based on MCG3/3.

3.2.6. Source of Errors. There are many possible sources of errors in this kind of calculation. These include (a) incomplete treatment of electron correlation, (b) torsional anharmonicity, especially the effective reduced moment of inertia, (c) coupling between vibration and rotation, and (d) more accurate treatment of coupled reaction-coordinate motion. We will now briefly consider these four sources of possible error:

(a) We have treated the electronic structure by direct dynamics at the MCG3/3 level. The direct dynamics scheme eliminates errors due to interpolation and fitting, so any error due to electronic structure comes from the choice of level. The MCG3/3 level is the highest level of non-density-functional direct dynamics that has ever been applied to a reaction with seven or more atoms. A recent validation study[62] of MCG3/3 for hydrogen transfer reactions shows a mean unsigned error of 0.76 kcal/mol, as compared to 0.64 kcal/mol for CCSD(T)/aug-cc-pVTZ, which is sometimes considered the gold standard, but which is unaffordable for direct dynamics.

(b) The torsional treatment has been validated[54] against converged quantum mechanical vibrational−rotational partition functions for H_2O_2 and six isotopmers, which is the only molecule with a torsion for which such accurate calculations are available. The errors are dominated by uncertainties in the torsional reduced moment of inertia, and for the present problem that is essentially the only source of error. Unfortunately though, the $^{12}C/^{13}C$ KIE is very sensitive to the choice of moment of inertia. That is why the present study devoted so much effort to this aspect of the problem. The residual error is impossible to estimate but is partly reduced by our semiempirical adjustments of subsection 3.2.1.

(c) Vibration−rotation coupling[65] is hard to include, and its effect on reaction rates is very uncertain. It is an important topic for future study.

(d) Although we used the SCT tunneling approximation, we expect, based on direct dynamics calculations[66] with a lower-level potential surface, that optimized multidimensional tunneling[17,67] would not change the result for this reaction. On the basis of validation studies,[68−70] the estimated residual error in the rate constant due to tunneling is about 30% at room temperature. Most of this error should cancel out in the $^{12}C/^{13}C$ KIE; however, as seen in subsection 3.2.5, factors associated with a consistent treatment of near-threshold energies can make a differences of a few parts per thousand in the KIE.

4. Conclusions

The effects of the coordinate system and of the method used for evaluating the contribution of the torsional mode have been studied for the $OH + CH_4 \rightarrow H_2O + CH_3$ reaction and the corresponding $^{12}C/^{13}C$ kinetic isotope effects. It has been found that the Cartesian coordinate system does not yield physical frequencies along the MEP, resulting in the CVT dividing surface being near the saddle point and in little variational effect. Calculations with nonredundant and redundant internal coordinates show that the CVT dividing surface should fall on the reactant side of the saddle point and that there should be a significant variational effect. The nonredundant internal coordinate system yields less physical frequencies than the redundant internal coordinate system, resulting in a variational effect that is too large and a forward rate constant that is too small. It has been determined that a redundant set of internal coordinates, including coordinates that involve the donor and acceptor atoms and bypass the transferring hydrogen, is required to adequately model the system.

The KIE depends on the coordinate system, but the KIEs calculated with the redundant internal coordinate system suffer from a lack of precision. Therefore, a systematic correction has been determined and applied to the nonredundant internal coordinate results.

The method used to model the torsion plays a critical role for both the forward rate and the KIE. The free-internal-rotor partition function apparently yields more physical results than the hyperbolic tangent interpolation method for a hindered rotation that has a very low barrier height. The CH_3-H-OH transition state is in the free-internal-rotor limit for the temperature range being studied, so the free-internal-rotor partition function has been used for the torsional mode rather than an interpolatory partition function. The placement of the transferring hydrogen atom into one of the two rotating groups is required for the torsional methods, and the placement affects the partition functions, but it is not clear which partition is more physical.

Studies of the KIE indicate that the torsion motion is best approximated using a mix of the curvilinear and rectilinear torsional schemes with the CH_3-H_2O partitioning. This has been verified using the frequencies from normal-mode analysis at the transition states of the ^{12}C and ^{13}C systems to determine an approximate ratio of the free-internal-rotor partition functions of the torsional mode. Calculations using a correction for both the coordinate system and the torsion show that the MCG3/3(corrected) calculated KIEs are within approximately 1−2 ppt of the experimental values. The MCG3/3(H&H) method has been developed and yields results within experimental error. A temperature dependence of the KIE has been determined, and it is recommended for use in climate modeling until experimental measurements of the temperature dependence of the KIE become available.

Acknowledgment. This work is supported in part by the U. S. Department of Energy (Grant No. DOE-FG02-86ER13579).

Supporting Information Available: Additional tables and figures. This material is available free of charge via the Internet at http://pubs.acs.org.

References and Notes

(1) Hien, R.; Crutzen, P. J. *Global Biogeochem. Cycles* **1997**, *11*, 43.

(2) McCarthy, M. C.; Boering, K. A.; Rice, A. L.; Tyler, S. C.; Connell, P.; Atlas, E. *J. Geophys. Res. D* **2003**, *108*, 4461.

(3) Cantrell, C. A.; Shetter, R. E.; McDaniel, A. H.; Calvert, J. G.; Davidson, J. A.; Loew, D. C.; Tyler, S. C.; Cicerone, R. J.; Greenbert, J. P. *J. Geophys. Res. D* **1990**, *95*, 22455.

(4) Saueressig, G.; Crowley, J. N.; Bergamaschi, P.; Brühl, C.; Brenninkmeijer, C. A. M.; Fischer, H. J. *J. Geophys. Res. D* **2001**, *106*, 23127.

(5) McCarthy, M. C.; Connell, P.; Boering, K. A. *Geophys. Res. Lett.* **2001**, *28*, 3567.

(6) Gupta, M. L.; McGrath, M. P.; Cicerone, R. J.; Rowland, F. S.; Wolfsberg, M. *Geophys. Res. Lett.* **1997**, *24*, 2761.

(7) Lin, H.; Zhao, Y.; Ellingson, B. A.; Pu, J.; Truhlar, D. G. *J. Am. Chem. Soc.* **2005**, *127*, 2830.

(8) Sellevag, S. R.; Nyman, G.; Nielsen, C. J. *J. Phys. Chem A* **2006**, *110*, 141.

(9) Pitzer, K. S. *J. Chem. Phys.* **1946**, *14*, 239.

(10) Pitzer, K. S. *Quantum Chemistry*; Prentice-Hall: Englewood Cliffs, NJ, 1953.

(11) Pitzer, K. S.; Gwinn, W. D. *J. Chem. Phys.* **1942**, *10*, 428.

(12) Truhlar, D. G.; Isaacson, A. D.; Garret, B. C. In *Theory of Chemical Reaction Dynamics*; Baer, M., Ed.; CRC Press, Boca Raton: FL, 1985; Vol. 3; p 65.

(13) Fernandez-Ramos, A.; Ellingson, B. A.; Garrett, B. C.; Truhlar, D. G. In *Reviews in Computational Chemistry*; Lipkowitz, K. B., Cundari, T. R., Eds.; Wiley-VCH: Hoboken, NJ, 2007; Vol. 23; p 125.

(14) Baldridge, K. K.; Gordon, M. S.; Steckler, R.; Truhlar, D. G. *J. Phys. Chem.* **1989**, *93*, 5107.

(15) Gonzalez-Lafont, A.; Truong, T. N.; Truhlar, D. G. *J. Phys. Chem.* **1991**, *95*, 4618.

(16) Truong, T. N.; Lu, D.-h.; Lynch, G. C.; Liu, Y.-P.; Melissas, V. S.; Stewart, J. J. P.; Steckler, R.; Garrett, B. C.; Isaacson, A. D.; Gonzalez-Lafont, A.; Rai, S. N.; Hancock, G. C.; Joseph, T.; Truhlar, D. G. *Comput. Phys. Commun.* **1993**, *75*, 143.

(17) Liu, Y.-P.; Lu, D.-h.; Gonzalez-Lafont, A.; Truhlar, D. G.; Garrett, B. C. *J. Am. Chem. Soc.* **1993**, *115*, 7806.

(18) Truhlar, D. G. Direct dynamics method for the calculation of reaction rates. In *The Reaction Path in Chemistry: Current Approaches and Perspectives*; Heidrich, D., Ed.; Understanding Chemical Reactivity 16; Kluwer Academic Publishers: Dordrecht: The Netherlands, 1995; pp 229−255.

(19) Rossi, I.; Truhlar, D. G. *Chem. Phys. Lett.* **1995**, *233*, 231.

(20) Srinivasan, J.; Allison, T. C.; Schwenke, D. W.; Truhlar, D. G. *J. Phys. Chem. A* **1999**, *103*, 1487.

(21) Pu, J.; Truhlar, D. G. *J. Chem. Phys.* **2002**, *116*, 1468.

(22) Isaacson, A. D.; Truhlar, D. G. *J. Chem. Phys.* **1982**, *76*, 1380.

(23) Lynch, B. J.; Truhlar, D. G. *J. Phys. Chem. A* **2003**, *107*, 3898.

(24) Fast, P. L.; Sanchez, M. L.; Truhlar, D. G. *Chem. Phys. Lett.* **1999**, *306*, 407.

(25) Zhao, Y.; Lynch, B. J.; Truhlar, D. G. *J. Phys. Chem. A* **2004**, *108*, 4786.

(26) Lynch, B. J.; Fast, P. L.; Harris, M.; Truhlar, D. G. *J. Phys. Chem. A* **2000**, *104*, 4811.

(27) Lynch, B. J.; Zhao, Y.; Truhlar, D. G. *J. Phys. Chem. A* **2003**, *107*, 1384.

(28) Zhao, Y.; Lynch, B. J.; Truhlar, D. G. *J. Phys. Chem. A* **2004**, *108*, 2715.

(29) Zhao, Y.; Truhlar, D. G. *Theor. Chem. Acc.* [Online early access]. DOI: 10.1007/s00214-007-0310-x. Published Online: July 12, 2007.

(30) Pople, J. A.; Head-Gordon, M.; Raghavachari, K. *J. Chem. Phys.* **1987**, *87*, 5968.

(31) Hehre, W. J.; Radom, L.; Schleyer, P. R.; Pople, J. A. *Ab Initio Molecular Orbital Theory*; Wiley: New York, 1986.

(32) Szabo, A.; Ostlund, N. S. *Modern Quantum Chemistry: Introduction to Advanced Electronic Structure Theory*; Dover Publications: Mineola, NY, 1996.

(33) Zhao, Y.; Rodgers, J. M.; Lynch, B. J.; Gonzalez-Garcia, N.; Fast, P. L.; Pu, J.; Ellingson, B. A.; Truhlar, D. G. *MULTILEVEL*, version 4.2; University of Minnesota: Minneapolis, MN, 2006.

(34) Frisch, M. J.; Trucks, G. W.; Schlegel, H. B.; Scuseria, G. E.; Robb, M. A.; Cheeseman, J. R.; Montgomery, J. A., Jr.; Vreven, T.; Kudin, K. N.; Burant, J. C.; Millam, J. M.; Iyengar, S. S.; Tomasi, J.; Barone, V.; Mennucci, B.; Cossi, M.; Scalmani, G.; Rega, N.; Petersson, G. A.; Nakatsuji, H.; Hada, M.; Ehara, M.; Toyota, K.; Fukuda, R.; Hasegawa, J.; Ishida, M.; Nakajima, T.; Honda, Y.; Kitao, O.; Nakai, H.; Klene, M.; Li, X.; Knox, J. E.; Hratchian, H. P.; Cross, J. B.; Bakken, V.; Adamo, C.; Jaramillo, J.; Gomperts, R.; Stratmann, R. E.; Yazyev, O.; Austin, A. J.; Cammi, R.; Pomelli, C.; Ochterski, J. W.; Ayala, P. Y.; Morokuma, K.; Voth, G. A.; Salvador, P.; Dannenberg, J. J.; Zakrzewski, V. G.; Dapprich, S.; Daniels, A. D.; Strain, M. C.; Farkas, O.; Malick, D. K.; Rabuck, A. D.; Raghavachari, K.; Foresman, J. B.; Ortiz, J. V.; Cui, Q.; Baboul, A. G.; Clifford, S.; Cioslowski, J.; Stefanov, B. B.; Liu, G.; Liashenko, A.; Piskorz, P.; Komaromi, I.; Martin, R. L.; Fox, D. J.; Keith, T.; Al-Laham, M. A.; Peng, C. Y.; Nanayakkara, A.; Challacombe, M.; Gill, P. M. W.; Johnson, B.; Chen, W.; Wong, M. W.; Gonzalez, C.; and Pople, J. A. *Gaussian 03*, revision C.02; Gaussian, Inc.: Wallingford, CT, 2004.

(35) Zhao, Y.; Schultz, N. E.; Truhlar, D. G. *J. Chem. Theory Comput.* **2006**, *2*, 364.

(36) Zhao, Y.; Truhlar, D. G. *MN-GFM*; version 3.0; University of Minnesota: Minneapolis, MN, 2006.

(37) Parthiban, S.; Martin, J. M. L. *J. Chem. Phys.* **2001**, *114*, 6014.

(38) Boese, A. D.; Martin, J. M. L. *J. Chem. Phys.* **2004**, *121*, 3405.

(39) Corchado, J. C.; Chuang, Y.-Y.; Fast, P. L.; W.-P., H.; Liu, Y.-P.; Lynch, G. C.; Nguyen, K. A.; Jackels, C. F.; Fernandez-Ramos, A.; Ellingson, B. A.; Lynch, B. J.; Melissas, V. S.; Villa, J.; Rossi, I.; Coitino, E. L.; Pu, J.; Albu, T. V.; Steckler, R.; Garrett, B. C.; Isaacson, A. D.; Truhlar, D. G. *POLYRATE*, version 9.6; Univeristy of Minnesota: Minneapolis, MN, 2007.

(40) Pu, J.; Corchado, J. C.; Lynch, B. J.; Fast, P. L.; Ellingson, B. A.; Truhlar, D. G. *MULTILEVELRATE*, version 9.4; University of Minnesota: Minneapolis, MN, 2006.

(41) Corchado, J. C.; Chuang, Y.-Y.; Coitino, E. L.; Ellingson, B. A.; Truhlar, D. G. *GAUSSRATE*, version 9.6; University of Minnesota: Minneapolis, MN, 2007.

(42) Melissas, V. S.; Truhlar, D. G.; Garrett, B. C. *J. Chem. Phys.* **1992**, *96*, 5758.

(43) Garrett, B. C.; Truhlar, D. G. *J. Phys. Chem.* **1979**, *83*, 1079.

(44) Pollak, E.; Pechukas, P. J. *J. Am. Chem. Soc.* **1978**, *100*, 2992.

(45) Fernández-Ramos, A.; Ellingson, B. A.; Meana-Pañeda, R.; Marques, J. M. C.; Truhlar, D. G. *Theor. Chem. Acc.* [Online early access]. DOI: 10.1007/s00214-007-0328-0. Published Online: July 11, 2007.

(46) Liu, Y.-P.; Lynch, G. C.; Truong, T. N.; Lu, D. h.; Truhlar, D. G.; Garrett, B. C. *J. Am. Chem. Soc.* **1993**, *115*, 2408.

(47) Jackels, C. F.; Gu, Z.; Truhlar, D. G. *J. Chem. Phys.* **1995**, *102*, 3188.

(48) Nguyen, K. A.; Jackels, C. F.; Truhlar, D. G. *J. Chem. Phys.* **1996**, *104*, 6491.

(49) Garrett, B. C.; Truhlar, D. G. *J. Chem. Phys.* **1982**, *76*, 1853.

(50) Tishchenko, O.; Truhlar, D. G. *J. Phys. Chem. A* **2006**, *110*, 13530.

(51) Martin, J. M. L. *J. Chem. Phys.* **1992**, *97*, 5012.

(52) Wilson, E. B.; Decius, J. C.; Cross, P. C. *Molecular Vibrations*; McGraw-Hill: New York, 1955.

(53) Truhlar, D. G. *J. Comput. Chem.* **1991**, *12*, 266.

(54) Ellingson, B. A.; Lynch, V. A.; Mielke, S. L.; Truhlar, D. G. *J. Chem. Phys.* **2006**, *125*, 84305.

(55) Chuang, Y.-Y.; Truhlar, D. G. *J. Chem. Phys.* **2000**, *112*, 1221.

(56) Chuang, Y.-Y.; Truhlar, D. G. *J. Phys. Chem. A* **1998**, *102*, 232.

(57) Natanson, G. A.; Garrett, B. C.; Truong, T. N.; Joseph, T.; Truhlar, D. G. *J. Chem. Phys.* **1991**, *94*, 7875.

(58) Villa, J.; Truhlar, D. G. *Theor. Chem. Acc.* **1997**, *97*, 317.

(59) Espinosa-Garcia, J.; Corchado, J. C. *J. Chem. Phys.* **2000**, *112*, 5731.

(60) Baulch, D. L.; Bowman, C. T.; Cobos, C. J.; Cox, R. A.; Just, T.; Kerr, J. A.; Pilling, M. J.; Stocker, D.; Troe, J.; Tsang, W.; Walker, R. W.; Warnatz, J. *J. Phys. Chem. Ref. Data* **2005**, *34*, 757.

(61) Demore, W. B.; Sander, S. P.; Golden, D. M.; Hampson, R. F.; Kurylo, M. J.; Howard, C. J.; Ravishankara, A. R.; Kolb, C. E.; Molina, M. J. In *Chemical Kinetics and Photochemical Data for Use in Stratospheric Modeling*; JPL Publication 92-20; Jet Propulsion Laboratory: Pasadena, CA, 1992.

(62) Zheng, J.; Zhao, Y.; Truhlar, D. G. *J. Chem. Theory Comput.* **2007**, *3*, 569.

(63) Joseph, T.; Steckler, R.; Truhlar, D. G. *J. Chem. Phys.* **1987**, *87*, 7036.

(64) Garrett, B. C.; Truhlar, D. G.; Grev, R. S.; Magnuson, A. W. *J. Phys. Chem.* **1980**, *84*, 1730.

(65) Garrett, B. C.; Truhlar, D. G. *J. Phys. Chem.* **1979**, *83*, 1915.

(66) Albu, T. V.; Corchado, J.; Truhlar, D. G. *J. Phys. Chem. A* **2001**, *105*, 8465.

(67) Fernandez-Ramos, A.; Truhlar, D. G. *J. Chem. Phys.* **2001**, *114*, 1491.

(68) Allison, T. C.; Truhlar, D. G. Testing the accuracy of practical semiclassical methods: Variational transition state theory with optimized multidimensional tunneling. In *Modern Methods for Multidimensional Dynamics Computations in Chemistry*; Thompson, D. L., Ed.; World Scientific: Singapore, 1998; pp 618−712.

(69) Pu, J.; Corchado, J. C.; Truhlar, D. G. *J. Chem. Phys.* **2001**, *115*, 6266.

(70) Pu, J.; Truhlar, D. G. *J. Chem. Phys.* **2002**, *117*, 1479.